Impact of Data Assimilation on Ocean Current Forecasts in the Angola Basin

Luke Phillipson[a,*], Ralf Toumi[a]

[a]*Space and Atmospheric Physics Group, Department of Physics, Imperial Collage London, London, UK*

Abstract

The ocean current predictability in the data limited Angola Basin was investigated using the Regional Ocean Modelling System (ROMS) with four-dimensional variational data assimilation. Six experiments were undertaken comprising a baseline case of the assimilation of salinity/temperature profiles and satellite sea surface temperature, with the subsequent addition of altimetry, OSCAR (satellite-derived sea surface currents), drifters, altimetry and drifters combined, and OSCAR and drifters combined. The addition of drifters significantly improves Lagrangian predictability in comparison to the baseline case as well as the addition of either altimetry or OSCAR. OSCAR assimilation only improves Lagrangian predictability as much as altimetry assimilation. On average the assimilation of either altimetry or OSCAR with drifter velocities does not significantly improve Lagrangian predictability compared to the drifter assimilation alone, even degrading predictability in some cases. When the forecast current speed is large, it found to be more likely that the combination improves trajectory forecasts. Conversely, when

*Corresponding author

Email address: l.phillipson14@imperial.ac.uk (Luke Phillipson)

the currents are weaker, it was found to be more likely that the combination degrades the trajectory forecast.
Keywords: Altimetry, Lagrangian data, Data assimilation, 4D-Var, Angola Basin, OSCAR

1. Introduction

Accurately forecasting regional ocean currents is of great importance for many applications including tracking ocean debris, planning search and rescue missions and responding to a major marine pollution event such as oil spills. Lagrangian trajectory forecasts are of particular importance for such applications and provide the most stringent test for an ocean model's circulation. Their challenging predictability is through the accumulation of errors including errors in the wind forcing, initial and boundary conditions, and approximations in model physics and sub-grid scale parameterizations [20]. Data assimilation (DA) is often applied to improve an ocean model's representation of the real circulation. This technique has subsequently contributed to a significant rise in forecast skill [43, 2]. Its objective is to derive an optimal estimate of the current and future state of the system using observations together with information from the dynamical model [23]. Many major ocean modelling systems have implemented DA schemes [16], including the Regional Ocean Modeling System [34], Nucleus for European Modeling of the Ocean [30], and Navy Coastal Ocean Model [50].

Despite advancements in the assimilation schemes themselves, ocean DA lags behind its atmospheric counterpart greatly regarding observations. The environment of the ocean means sampling is difficult, with satellite informa-

tion only limited to the surface [1]. Buoys, profiling floats (Argo), satellites, moorings, coastal radars, gliders and surface drifters make up the main observational data sets for the ocean.

This study focuses on three data sets that can have the strongest influence on the upper ocean velocity: satellite altimetry, satellite-derived surface currents and drifter data. Altimetry provides ocean velocity information indirectly through the geostrophy within the model. The assimilation of altimetry has been shown to improve model circulation in numerous studies of various parts of the ocean [18, 17, 16, 33, 13]. Satellite-derived surface current products compute the geostrophic component explicitly from altimetry often combining with a wind-induced Ekman surface current component derived from surface wind data. OSCAR is a widely used satellite-derived surface current analysis product [22] and has only been previously assimilated using a nudging technique for the Indian Ocean by Santoki et al. [47], where surface current improvements were demonstrated. Surface drifters sample numerous scales of the ocean circulation [27] and their assimilation has also been shown to improve model circulation and predictability [32, 39, 31, 38, 46, 37, 8]. The growing interest in predicting flow trajectories, due in part to the Deepwater Horizon incident, has led to a rise in the utilisation of drifters for improving forecasts [42]. Recent research on the assimilation of drifter velocities remains focussed on the Gulf of Mexico (GOM) due to a large amount of drifter data available. Muscarella et al. [35] and Carrier et al. [9] utilised the Grand Lagrangian Deployment (GLAD) data set (300 drifters released in a short period in a localised region in the GOM) and have shown that assimilating drifter inferred velocities improves both the Lagrangian predictability and

sea level forecast. Berta et al. [3] has combined GLAD drifters and altimetry in a Lagrangian - variational scheme to produce instantaneous estimates of ocean current velocities improving the hind-cast trajectory skill.

Our contribution focused on forecasting ocean velocities with ROMS and a 4D-Var DA scheme quantifying the relative importance of assimilating altimetry, OSCAR and limited drifter data separately and combined. Our approach was similar to that of Muscarella et al. [35] but differed in the following ways: Firstly, we sought to separately quantify the individual and combined use of altimetry, OSCAR and drifters. This was the first time OSCAR has been assimilated using an advanced data assimilation method such as 4D-Var. Besides the additional components added to the geostrophic velocities, OSCAR closely relates to altimetry, and whether the OSCAR assimilation provides any added benefit was not understood.

Secondly, our study focused on the Angola Basin with a limited number of drifters. The Angola Basin is part of the tropical ocean and therefore has crucial characteristics that differ from the GOM, such as a much larger Rossby Radius of deformation. The Angola basin was chosen due to its diverse ocean currents [52], importance as a petroleum reservoir [12], and marine biodiversity [5]. This study was the first application of data assimilation in the Angola Basin. Figure 1 shows a schematic of notable oceanographic features of the region. Major oceanic features include the Equatorial Under Current (EUC), Gabon-Congo Undercurrent (GCUC), South Equatorial Current (SEC), the South Equatorial Counter Current (SECC) which branches to become the Angola Current (AC) moving south along the coast, the Benguela Oceanic Current (BOC) and its coastal branch the Benguela Coastal Current (BCC)

moving north along the coast, the Angola dome (AD), the Angola-Benguela front (ABF) and the Congo River [52].

Furthermore, the Angola Basin has a limited drifter coverage. While the GOM and GLAD drifter data set remains a valuable case study, this abundance of observations constrained to a small region is not typical. In most other regions the drifter coverage would be substantially less, and in the case of a marine pollution, would likely require some form of targeted deployment [48]. Therefore this study focused on the impact of local changes near the drifters and not how information spreads to unobserved regions, with no data denial experiments performed. In a more realistic drifter limited region, the impact of assimilating the drifters together with common observations streams such as altimetry was not apparent.

The paper is organised as follows: Section 2 will present the numerical model, data assimilation scheme, observations, and methodology. Section 3 will present the results, and Section 4 will highlight the discussion, concluding in Section 5 with a summary.

2. Methodology

2.1. Numerical Model

ROMS is a hydrostatic, primitive equation, Boussinesq ocean general circulation model. Shchepetkin and McWilliams [49] describes an in-depth review of the numerics and formulation. Previous studies have utilised this model in understanding the Congo River plume dynamics [15] and effects on ocean temperature [56]. The model domain extends between $1^oS - 21^oS$ and $3.7^oE - 13.8^oE$ with a 10km resolution and 40 terrain-following verti-

cal levels. To determine the degree of vertical stretching, ROMS employs a generalised topography-following coordinate system with user-defined σ parameters. ROMS σ parameters were as follows: $h_c = 200m$ is the critical depth applied to both the surface and bottom boundary layer where there is enhanced resolution, and $\sigma_s = 10$ and $\sigma_b = 2$ control the degree of enhanced resolution at the surface and bottom boundary layer respectively. Thus, the vertical levels were compressed at the surface to increase the vertical resolution of the surface currents.

Sub-grid mixing was prescribed using the generic length-scale (GLS) scheme of Warner et al. [55]. Lateral boundary and initial conditions for temperature, salinity, ocean current velocities and sea surface height were obtained from the HYCOM reanalysis [10]. Atmospheric forcing at the surface for downward radiative surface fluxes, sea level pressure, 2m specific humidity, 2m air temperature, 10m winds, and total precipitation were obtained from European Centre for Medium-Range Weather Forecasts (ECMWF) reanalysis (ERA)-Interim reanalysis data (ERA-I) [14]. Several major rivers, namely the Nyanga, Kouilou, Kwanza (Cuanza), Kuene, and the Congo were included into the model. Following White and Toumi [56], river flow rates were obtained from various sources, including the RivDIS v1.1 database [54], the Global Environmental Monitoring System/Global River Inputs (GEMS/GLORI) database [29], the EIB ERE and the University of Brazzaville available at (`http://hmf.enseeiht.fr/travaux/CD0809/bei/beiere/groupe5/node/53`).

2.2. Assimilation scheme: IS4D-Var

The variational approach to data assimilation is to minimise a cost function to produce an optimal analysis. This cost function represents both the

misfit between the model and background state and the misfit between the model state and observations. For this study, we used incremental strong four-dimensional variational assimilation (IS4D-Var) adjusting initial conditions, surface forcing and boundary conditions. Moore et al. [34] describes a comprehensive outline of the numerical algorithms of ROMS IS4D-Var.

Before running ROMS 4D-Var, it is necessary to specify parameters in the background error covariances. The horizontal decorrelation length scale assigned to the initial condition background error covariance was 100 km. This was inferred from the approximate average of the Rossby radius of deformation for the region. Owing to the large latitudinal coverage for the domain, the Rossby radius of deformation ranges from approximately 60 km at 21^o S to 230 km at 1^o S [11]. 100 km was also chosen for the surface forcing and open boundary background error covariances. A model climatology run with no assimilation from 2004-2008 was used to estimate standard deviations for the initial condition and surface forcing background error covariances. HYCOM boundary conditions were used to estimate standard deviations for open boundary background error covariance.

Multivariate balance options for momentum (geostrophic balance) were not enforced. For the stability of domains boarding the equator, the equatorial adjustment of the geostrophic balance is required and has not yet been implemented into the ROMS 4D-Var balance. Instead, the tangent linear and adjoint models achieve multivariate characteristics as described by Carrier et al. [9].

Observational errors comprise of the measurement error, the error of representativeness, and some subjective adjustment to firstly, obtain the appro-

priate relative weightings and secondly, to inflate the impact of a limited number of observations [7]. The observation errors were assigned as follows: 0.04 ms^{-1} for drifter velocities, 0.12 ms^{-1} for OSCAR velocities, 1 °C for SST, 0.04 m for SSH, 0.1 °C for in situ T and 0.01 PSU for in situ S. While 0.04 ms^{-1} for the drifter velocities borders the limit of representativeness, we applied this as the absolute lower limit to inflate the impact of the assimilation of sparse data. OSCAR velocity errors were obtained from Johnson et al. [22]. In situ temperature and salinity profiles make up a small percentage of the assimilated variables and were the only observations that sample subsurface depths. Here we kept errors constant vertically for ease of implementation.

Prior specification of parameters controlling the convergence of the cost function was also required i.e. the number of inner and outer loops. After a series of sensitivity experiments (not shown), it was determined 25 inner loops and one outer loop was sufficient for the convergence of the cost function (reduced by a factor of 80-90%), as well as keeping computational costs low.

2.3. Lagrangian scheme

The ROMS online particle trajectory module was used to simulate drifter trajectories during the model forecast. This module uses a fourth-order Milne predictor and fourth-order Hamming corrector scheme to time-step the float trajectory [24]. To simulate the 15m drogue depth of the observed GDP drifters geopotential (fixed depth) floats were specified. Random walk (simulates sub-grid scale vertical diffusion) is also available in the ROMS float module but was not activated here for similar comparisons with other studies that only use advection (i.e. the forcing of the ocean currents alone). Clusters

of floats can be defined by the user with customizable distributions. To partially account for model error, a small localised cluster of 21 drifters centred on the exact location of the observed drifters of 4km width was utilised. The advantage of using the ROMS online module over the numerous offline options available [53] is that the time-stepping of the numerical particle scheme is of the same order as that of the model integration.

2.4. Observations

Satellite sea surface temperature (SST) and in situ temperate and salinity profiles (T&S) were included in this study as a baseline assimilation. Altimetry, OSCAR and drifter velocity observations were subsequently added to this baseline (separately and combined) to quantify the improvement. The study period (1st Jan - 14th March 2013) was chosen to maximise the coverage of drifter data within the domain.

SST observations were obtained from a blended analysis product, the NOAA $1/4^o$ daily Optimum Interpolation SST (daily OISST). This analysis combines observations from satellites such as the Advanced Very High Resolution Radiometer (AVHRR), ships and buoys [44].

In situ T&S profile observations were obtained from the EN4 dataset provided by the Met Office Hadley Centre [19]. This data set collates all types of ocean profiling instruments such as expendable bathythermographs (XBT), Argo floats, and Conductivity Temperature Depth (CTD) profiles from several data compilation sources including World Ocean Data (WOD09) and the Argo global data assembly centres (GDACs). Upon compilation, the data set is then subject to several quality control procedures.

Gridded sea surface height (SSHG) observations consisted of a merged

Ssalto/Duacs data-set (TOPEX/Poseidon, Jason-1&2, Envisat, ERS-1&2, and GFO measurements) distributed by Aviso with support from the Centre National dEtudes Spatiales (CNES). ROMS does not resolve the global steric signal. This signal was removed from SSHG using a database provided by Willis et al. [57]. Furthermore, SSHG was calibrated to ensure ROMS and AVISO dynamic topography were spatially and temporally equal on a long-term average.

Ocean Surface Current Analysis Real-time (OSCAR) is a surface current analysis product. The analysis combines geostrophic, Ekman, and Stommel shear dynamics along with a term from the surface buoyancy gradient [6]. These terms were estimated from satellites observing SSH from TOPEX/Poseidon, surface vector winds from the Special Sensor Microwave Imager (SSM/I), and SST from the Advanced Very High Resolution Radiometer (AVHRR). Bonjean and Lagerloef [6] provides an in-depth formulation of the model used to construct the analysis. The resulting gridded analysis is of $1/3^{\circ}$ resolution and represents the mean of the upper 30 m ocean currents. We assimilated OSCAR at a depth of 15 m and every five days as per the temporal resolution. By construction, OSCAR and SSHG partially use the same information (TOPEX/Poseidon) and so are not truly independent.

Surface current velocity observations were obtained from Surface Velocity Program (SVP) drifters maintained by the Global Drifter Program's (GDP) Drifter Data Assembly Centre [40]. These velocities have been derived from 6 hourly interpolated drifter positions and centred finite differences. The drifters have a drogue set at a depth of 15 m. Figure 2 shows the drifter

trajectories over the study period. Note the drifters are roughly evenly distributed throughout the domain although the majority remains away from the coast. Positions and velocities for all drifters were smoothed using a 24 hour 6th order low-pass Butterworth filter to eliminate tidal currents [45].

2.5. Data Assimilation experiments

Assimilation was performed sequentially for six experiments starting on 1 Jan 2013 (initialized from a one year model spin up without assimilation) using four-day assimilation windows ending on 10th March (17 cycles) adjusting the initial conditions, surface forcing and boundaries conditions (Table 1). Prior initial conditions for each cycle were obtained from the final posterior analysis from the previous cycle, except for the first DA cycle in which all experiments were initialised from HYCOM data. The prior boundary conditions and surface forcing were from HYCOM and ERA-I. Alongside the assimilation cycles, a series of four-day forecast cycles were run starting from the end of every DA cycle to assess the short-term forecast skill of the model.

The first experiment was the assimilation of the baseline observations, SST and T&S profiles. This represents a standard observational data set often assimilated in operational forecast centres that only have a marginal impact on the upper ocean current circulation. The subsequent five experiments were the addition of two combinations of altimetry or OSCAR and drifters, and each observation individually to the baseline. This study was the first to show the individual impacts alongside the combination of these datasets.

To assess the performance of the assimilation system, a normalised error metric was used [8, 13], described here as:

Table 1: Summary of the DA experiments. *X* indicates the experiment was assimilating the corresponding observational data set. DRIFT is the drifter inferred velocities, SSHG is altimetry, OSCAR is the analysis surface currents, SST is satellite sea surface temperature, and TS are profile measurements of temperature and salinity. B refers to the baseline observational dataset to which additional observations are added.

Exp. Name	OSCAR	DRIFT	SSHG	SST	TS
TS-SST (B)				X	X
B-SSHG			X	X	X
B-OSCAR	X			X	X
B-DRIFT		X		X	X
B-SSHG-DRIFT		X	X	X	X
B-OSCAR-DRIFT	X	X		X	X

$$J_{fit} = \frac{1}{N} \sum_{n=1}^{N} \frac{|y_n - H_n X_a|}{\sigma_n} \quad (1)$$

where y_n is the nth observation; X_a is the model analysis mapped to the observations location by H_n, the observation operator; and σ_n is the error standard deviation of the nth observation. J_{fit} represents a unit-less measure of the fit of the observations to the model information within one standard deviation of the observation error. If J_{fit} is less than 1, then the analysis residual is, on average, within observation error bounds.

To assess the performance of the forecast, simulated floats were released into the ROMS (see Section 2.3) at the start of every new forecast cycle. Outside assimilation cycles, drifter observations become approximately independent for the subsequent forecast cycles. Four days was assumed to be adequate length for approximate independence between assimilated and observed data.

With the computed float trajectories, four skill metrics were used to assess the Lagrangian predictability (Table 2): average separation distance after 24 hours between the drifters and ROMS simulated floats; the average growth rate of separation distances (linear fit applied to the average separation distances over the entire 4 day forecast); an average angular difference after 24 hours [35], and a normalized 3 day cumulative distance difference skill score i.e. the ratio of the cumulative separation between drifters and simulated floats and cumulative distance travelled by the observed drifter after 3 days [25].

Table 2: Summary of Lagrangian metrics used within the study. $x_{obs}(t)$ represents the longitudinal and $y_{obs}(t)$ the latitudinal position at time t (hours) for the observed drifter and $x_{ROMS}(t)/y_{ROMS}(t)$ for the ROMS simulated floats. $ang_{obs}(t)$ represents the angle between the starting position and position at time, t for the observations and $ang_{ROMS}(t)$ for ROMS simulated floats.

Metric	**Equation**
Separation Distance $D(t)$	$\sqrt{[x_{obs}(t) - x_{ROMS}(t)]^2 + [y_{obs}(t) - y_{ROMS}(t)]^2}$
Growth Rate of Separation Distance $D_{Linear}(t_0..t_{end})$	$D(t_0..t_{end})/(t_0..t_{end})$
Angular Difference $AD(t)$	$ang_{obs}(t) - ang_{ROMS}(t)$
Cumulative Distance Difference Skill Score $S(t_{end})$	$S = \begin{cases} 1-c, (c<1) \\ 0, (c>1) \end{cases}$ $c(t_{end}) = \sum D(t_0..t_{end})/\sum D_0((t_0..t_{end}))$ $D_0(t) = \sqrt{[x_{obs}(t) - x_{obs}(t-1)]^2 + [y_{obs}(t) - y_{obs}(t-1)]^2}$

3. Results

3.1. Validation of the assimilation system

The asymptote of the cost function was reached before the 25 iterations of the inner loops and one outer loop. Over the entire study period, the cost function reduced on average by approximately 93%. The true non-linear cost function reduced on average by 80%, which suggests that the tangent linear assumption held well over the four day assimilation windows.

Table 3: The average J_{fit} of each analysis cycle (17) over the four days. Significant improvements over TS-SST (B) are shown in bold.

Exp. Name	OSCAR-U | V	DRIFT-U | V	SSH	SST	In-Situ T	In-Situ S
CONTROL	0.95 | 0.92	3.12 | 2.59	0.71	1.23	7.43	14.89
TS-SST (B)	0.99 | 1.01	3.23 | 3.01	0.98	0.23	2.25	4.73
B-SSHG	**0.78 | 0.80**	**2.65 | 2.44**	**0.27**	0.24	2.32	5.17
B-OSCAR	**0.56 | 0.52**	**2.57 | 2.42**	**0.76**	0.22	2.22	5.22
B-DRIFT	0.98 | 1.00	**1.08 | 0.98**	0.96	0.24	2.49	5.56
B-SSHG-DRIFT	**0.83 | 0.81**	**1.04 | 0.96**	**0.29**	0.25	2.63	6.13
B-OSCAR-DRIFT	**0.58 | 0.53**	**1.24 | 1.20**	**0.76**	0.22	2.19	5.06

The baseline experiment (TS-SST) improved the fit over the control in all three observations that were assimilated. da Rocha Fragoso et al. [13] commented on the challenge of assimilating in-situ T and S, often leading to high values of J_{fit} as also seen here.

J_{fit} reduced either below or close to 1 in each experiment for each observation that was assimilated (black bold in Table 3). The assimilation system

was therefore on average, fitting each observation within the observational error bounds.

The most significant J_{fit} improvements beyond non-assimilated observations were confined to experiments assimilating remotely sensed observations, B-SSHG and B-OSCAR. For example, drifter velocities were not assimilated in B-SSHG, but a small decrease in drifter velocity J_{fit} was exhibited over the baseline by approximately 15 %. However, the assimilation of drifter velocities (B-DRIFT) improved the fit to the non-assimilated SSHG observations locally, decreasing the SSH J_{fit} by approximately 11% within 1° of the assimilated drifters. The drifters in this study were too sparse to impact the domain-wide SSH J_{fit} statistics (Table 3).

In addition to J_{fit}, a more qualitative assessment of the performance of an assimilation system is the increment fields (posterior circulation minus the prior circulation). Figure 3 shows the assimilation prior, posterior and increment of the model SSH averaged over the 1st assimilation cycle (1st to 5th January 2013) with overlaying velocity vectors for experiments B-SSHG and B-DRIFT. Highlighted in B-DRIFT are the drifters available for assimilation in the first cycle.

The prior circulation captured the coastal current (GUCU), however overestimated the strength and size of an anti-cyclonic eddy. From AVISO (not shown), this eddy slowly evolved east to west over the span of a few months. The assimilation of SSHG corrected this by weakening a strong anti-cyclonic eddy at around 10 °S, 11 °E while strengthening another further south, shifting the positions as well as the size. The B-DRIFT assimilation similarly achieved these two critical adjustments with only four drifters, demonstrat-

ing how the assimilation of a small amount of Lagrangian data can have a relatively large spatial influence, although this is highly dependent on the assigned decorrelation length. Nevertheless, the drifters within this cycle were still too few to constrain the entire domain creating spurious adjustments elsewhere. As the coverage of drifters increased with time (4 to 16), the SSHG J_{fit} for B-DRIFT improved (Figure 4). However, beyond cycle 9, J_{fit} rapidly degraded. This is likely due to the emergence of an isolated drifter, north of 5 °S. This drifter is in a critical area where the GUCU is strong (Figure 1) and again cannot sufficiently constrain larger scales.

3.2. Forecast Skill

The 17 four day forecasts were assessed to understand how well the adjustments made to the initial conditions by the assimilation system (Table 3) were maintained. Standard metrics used to evaluate the forecast accuracy included the time average root mean squared error (RMSE), correlation coefficient (R) and the average RMSE percentage increase by the end of the forecast window.

Similar to the J_{fit} statistics, the average forecast RMSE reduced in each experiment for each observation that was assimilated (black bold in Table 4). Therefore, the forecasts on average maintained the memory of the initial adjustments made by the assimilation over the four days.

Interestingly, the average RMSE for OSCAR velocities in the B-OSCAR forecasts were larger than that in the B-SSHG forecasts, by approximately 0.8 cms^{-1}. The average RMSE % increase was also slightly larger by 3 %.

Again as in the J_{fit} statistics, B-SSHG and B-OSCAR were the most significantly improved forecasts for non-assimilated observations, such as re-

Table 4: The average RMSE (cms^{-1} for OSCAR and drifter velocites, cm for SSH, °C for SST and in-situ T, and PSU for in-situ S) of each forecast cycle (17) over the four days. Significant improvements over TS-SST (B) are shown in bold.

Exp. Name	OSCAR-U | V	DRIFT-U | V	SSH	SST	In-Situ T	In-Situ S
CONTROL	15.3 | 14.4	15.5 | 13.2	3.5	1.36	1.08	0.23
TS-SST (B)	15.8 | 15.9	16.2 | 15.0	4.5	0.63	0.87	0.19
B-SSHG	**14.1 | 13.2**	**13.4 | 12.5**	**2.3**	0.62	0.89	0.20
B-OSCAR	**14.7 | 14.0**	**13.6 | 13.0**	**3.5**	0.62	0.82	0.20
B-DRIFT	15.8 | 16.2	**12.4 | 12.0**	4.4	0.63	0.91	0.20
B-SSHG-DRIFT	**14.6 | 13.6**	**11.1 | 10.7**	**2.4**	0.63	0.91	0.21
B-OSCAR-DRIFT	**14.5 | 14.0**	**11.7 | 11.6**	**3.5**	0.61	0.82	0.20

ducing the RMSE for drifter velocities by approximately 17-20%. B-DRIFT forecasts only exhibited RMSE improvements locally to the SSH (5%) and OSCAR (6%).

The average R is similar to the RMSE and J_{fit} statistics (Table 6), except that the B-DRIFT forecast exhibited a domain-wide improvement in the R of OSCAR velocities and not just locally. This improvement indicates that the drifters are more able to improve eddy and ocean current locations and directions rather than the absolute magnitudes. This is demonstrated in Figure 5 showing ocean current velocities for OSCAR observations, and the baseline TS-SST (B) and B-DRIFT forecast, averaged over the entire study period. The OSCAR observations show three distinct dynamical features; a strong coastal current forming part of the Gabon-Congo Undercurrent (GCUC) which feeds the Angola Current (AC), a large semi-persistent

Table 5: The average RMSE (%) increase of each forecast cycle (17) after 4 days with respect to the initial forecast RMSE.

Exp. Name	OSCAR-U | V	DRIFT-U | V	SSH
B-SSHG	9% | 10%	10% | 9%	100%
B-OSCAR	12% | 13%	12% | 13%	11%
B-DRIFT	1% | 1%	113% | 109%	−1%
B-SSHG-DRIFT	8% | 10%	139% | 111%	100%
B-OSCAR-DRIFT	10% | 13%	76% | 100%	10%

anti-cyclonic eddy at 11°S 8°E spanning approximately 200 km and three strong zonal currents from 13°S to 21°S. While these features are present in the TS-SST forecasts, the eddy location is erroneously shifted by 3°N. Although the size is greatly reduced, the addition of the drifters (B-DRIFT) improved the predicted location of the dominant eddy, correctly shifting the position southwards.

3.3. Drifters

Trajectory forecasts serve as a stringent test of a model's ability to accurately forecast ocean currents. Figure 6 gives an example of such trajectory forecasts for each experiment from the 22nd to 26th February 2013 (forecast cycle 13). Black lines represent the observed trajectory, and red lines (crossed lines in-print) represent the simulated float. A smaller section from the main

Table 6: The average R of each forecast cycle (17) over the four days. Significant improvements over TS-SST (B) are shown in bold.

Exp. Name	OSCAR-U | V	DRIFT-U | V	SSH	SST	In-Situ T	In-Situ S
CONTROL	0.14 | 0.09	0.10 | 0.29	0.83	0.95	0.99	0.91
TS-SST (B)	0.19 | 0.10	0.11 | 0.27	0.85	0.98	0.99	0.94
B-SSHG	**0.31 | 0.28**	**0.40 | 0.41**	**0.96**	0.98	0.99	0.92
B-OSCAR	**0.24 | 0.22**	**0.29 | 0.32**	**0.88**	0.98	0.99	0.93
B-DRIFT	**0.25 | 0.16**	**0.48 | 0.52**	0.84	0.98	0.99	0.92
B-SSHG-DRIFT	**0.30 | 0.27**	**0.56 | 0.52**	**0.96**	0.98	0.99	0.92
B-OSCAR-DRIFT	**0.28 | 0.24**	**0.46 | 0.47**	**0.88**	0.98	0.99	0.93

domain highlights five drifters, and their difference from the simulated ROMS floats.

The B-SSHG-DRIFT forecast best represented Drifters 1 and 2. For Drifter 1, the B-SSHG forecast predicted the position of the eddy too far west. For the B-DRIFT forecast, a larger current created from the assimilation of Drifter 2 was erroneously influencing the local region of Drifter 1. However, when combined in B-SSHG-DRIFT, the eddy was more pronounced, with Drifter 1 correctly positioned on the northern edge. For Drifter 2 both the B-SSHG and B-DRIFT forecasts were able to capture the correct direction of the strongest current but only the combination correctly captured the along track speed.

Drifters 3 and 4 show that this interaction was not always beneficial with a degradation of the forecast as compared to B-DRIFT. For Drifter 3, the B-SSHG-DRIFT forecast had spurious southward flow while for Drifter 4,

the position of the eddy was forecast too far north. Both these drifters were situated in weaker currents where the assimilation tends to change the boundaries of the larger currents in proximity. Here, we have shown a possible preference for the combination with altimetry (B-SSHG-DRIFT) or individual assimilation of drifter observations (B-DRIFT).

Finally, Drifter 5 was best represented by the B-OSCAR-DRIFT forecast. Here, the B-OSCAR forecast exhibited some skill for Drifter 5 and in combining with the drifters improved the skill further by correctly shifting the boundary of current. For this example, we have shown how B-DRIFT, B-SSHG-DRIFT and B-OSCAR-DRIFT can each provide unique local improvements producing the best trajectory forecast for their particular drifter.

For all simulated ROMS trajectories, the Lagrangian predictability was assessed quantitatively using the four skill metrics (Table 2). Table 8 summarises the average values of each metric in all the experiments. Two-sample Kolmogorov-Smirnov tests were performed in all experiments to test the significance between distributions. $p < 0.05$ indicates that the null hypothesis (the two samples come from the same distribution) is rejected. The KS test is a non-parametric test which is necessary for skewed data samples Massey Jr [28].

Averaged over the entire study period, the experiments with the smallest average separation distance between the simulated trajectories and the observed drifter trajectories after 24 hours $\hat{D}(24)$, were B-DRIFT and B-SSHG-DRIFT, both at 9.5 km. In comparison to the baseline forecast TS-SST (B) this was an average improvement of 6.8 km (42%) in predictability after 24 hours. B-OSCAR-DRIFT closely followed this with an improvement

Table 7: Summary of Lagrangian metric statistics. For $\hat{D}(24)$ and $D_{Linear}(0..96)$ mean values are displayed with the interquartile range in brackets. For $AD(24)$ the mean value is displayed with standard deviation.or both $S(72)$ $n = 1$ and $n = 2$ the mean values are displayed with percentage of positive value skill scores in square brackets.

Metric	CONTROL	TS-SST (B)	B-SSHG	B-OSCAR	B-DRIFT	B-SSHG-DRIFT	B-OSCAR-DRIFT
$\hat{D}(24)$ (km)	15.3 (11.1)	16.3 (12.4)	13.4 (10.2)	13.5 (9.4)	9.5 (8.2)	9.5 (7.0)	9.9 (8.6)
$D_{Linear}(0..96)$ (km/day)	13.5 (11.4)	14.1 (10.6)	10.9 (8.6)	10.7 (7.1)	8.7 (6.8)	8.3 (5.1)	8.2 (5.8)
$AD(24)$ (*degrees*)	5 ± 92	-5 ± 94	12 ± 83	10 ± 84	7 ± 54	15 ± 62	7 ± 63
$S(72)$ $n = 1$	0.16 [45%]	0.13 [44%]	0.24 [58%]	0.22 [60%]	0.35 [77%]	0.35 [75%]	0.36 [82%]
$S(72)$ $n = 2$	0.42 [79%]	0.41 [81%]	0.51 [87%]	0.51 [90%]	0.61 [93%]	0.62 [93%]	0.62 [94%]

of 6.4 km (40%), while B-SSHG and B-OSCAR also exhibited significant improvements, though only by less than half as much (17%). The differences between B-DRIFT, B-SSHG-DRIFT and B-OSCAR-DRIFT $\hat{D}(24)$ distributions were not significant ($p = 0.4$), nor were B-SSHG and B-OSCAR $\hat{D}(24)$ distributions ($p = 0.6$).

Similar to Muscarella et al. [35], we applied a linear fit to the mean separation distances giving the average growth rate in separation per day $D_{Linear}(0..96)$.

The experiment with the smallest average separation growth rate $D_{Linear}(0..96)$ was B-OSCAR-DRIFT with a rate of 8.2 km/day, an average improvement of 5.9 km/day (42%) over the baseline (Figure 7). B-SSHG-DRIFT and B-DRIFT closely followed this with an improvement of 5.8 km/day (41%) and 5.4 km/day (38%). Similar to $\hat{D}(24)$, the differences between these $D_{Linear}(0..96)$ distributions were not significant ($p = 0.35$). $D_{Linear}(0..96)$ for B-SSHG and B-OSCAR was 10.9 and 10.7 km/day, an average improvement of 3.2 and 3.4 km/day ($\approx 23\%$). While these averages were similar, the

inter-quartile range differed by as much as 1.5 km/day. This difference can be seen graphically by a more compact group of grey lines representing the average $D_{Linear}(0..96)$ for each cycle (Figure 7).

The angular differences between each observed 24-hour drifter angle (the angle between the starting position and position after 24 hours) and 24-hour simulated trajectory angle within each forecast is shown in Figure 8. Since the spread was much larger for $AD(24)$ than previous metrics, it was useful to note improvements regarding the reduction of the standard deviation in $AD(24)$.

The experiment with the smallest standard deviation of the angular difference $AD(24)$ was B-DRIFT with 54°, an average improvement of 40 ° (43%) over the baseline. B-SSHG-DRIFT and B-OSCAR-DRIFT closely followed this with a mean improvement of 32 ° and 33 ° (34%). Again, similar to the previously discussed metrics the differences between these $AD(24)$ distributions were not significant ($p = 0.26$).

The standard deviation of $AD(24)$ for B-SSHG and B-OSCAR was 83° and 84°, an average improvement of 11° and 10° (12%). This improvement was approximately four times smaller than for B-DRIFT, the largest difference between B-SSHG and B-DRIFT for any of the Lagrangian metrics. The assimilation of drifters is valuable for correcting the angle of the local currents.

For the normalised three-day cumulative distance difference skill score $S(72)$, B-OSCAR-DRIFT had the largest skill score on average at 0.36, an average improvement of 0.23 (176%) over TS-SST (B). B-DRIFT and B-SSHG-DRIFT closely followed this with an average improvement of 0.22

(169%). It was expected that forecast evaluation would likely yield lower skill scores [25] than for analysis evaluation such as used by Berta et al. [4] and Liu et al. [26]. The threshold number, n (see Table 2) can be increased to compensate for increased forecast error. For increased threshold ($n = 2$) average cumulative skill score for B-OSCAR-DRIFT, B-SSHG-DRIFT and B-DRIFT was 0.62 and 0.61, an average improvement of 0.21 and 0.20 (50%) over TS-SST (B). Again, the differences between these $S(72)$ distributions were not significant ($p = 0.93$). The increased threshold ($n = 2$) average cumulative skill score for B-SSHG and B-OSCAR was 0.51, an average improvement of 0.1 (25%).

Unique to $S(72)$, the percentage of positive value skill scores can be assessed. This positive value percentage ($n = 1$) increases the most in B-OSCAR-DRIFT by 38%, followed by B-DRIFT by 32%, B-SSHG-DRIFT by 31%, B-OSCAR by 16% and B-SSHG by 14%. This indicates that previously simulated drifters with no skill ($S(72) = 0$) can now be assigned skill with the assimilation of altimetry and OSCAR and more substantially by the addition of drifters.

The spatial distributions of all Lagrangian metrics were independent of location (not shown).

3.3.1. Dependence on current speed

To further investigate B-SSHG-DRIFT and B-DRIFT forecast skill differences, improvements or degradation were categorised into the percentage of positive and negative values of the difference of $D(t)$ between B-SSHG-DRIFT and B-DRIFT. Positive values correspond to cases when the B-SSHG-DRIFT forecast was more skilful than the B-DRIFT forecast. Con-

versely, negative values represent cases when the B-SSHG-DRIFT forecast was less skilful than the B-DRIFT forecast. Figure 10 shows the percentage difference between B-SSHG-DRIFT and B-DRIFT for the separation distance as a function of time. The red and blue lines represent faster and weaker currents based on the median of the observed drifter speed distribution (upper and lower 50%).

The difference between weaker and stronger current distributions become significant beyond 30 hours. At this point, the weaker currents distribution (blue line) stays around roughly 5% more B-DRIFT forecast improvements (negative values) and peaking early in the forecast around 38 hours at almost 15%. This is in contrast to the stronger currents distribution which steadily remains above 8% more B-SSHG-DRIFT forecast improvements (positive values) peaking at 88 hours at around 12%. Therefore, after 30 hours for weaker currents, it is more likely (5% to 15%) that the B-DRIFT forecast will outperform B-SSHG-DRIFT. While for stronger currents it is more likely (12%) that the B-SSHG-DRIFT forecast will outperform the B-DRIFT forecast. The same analysis was performed for metrics $AD(t)$ and $S(t)$ (not shown). The $AD(t)$ percentage difference between B-SSHG-DRIFT and B-DRIFT forecasts revealed no dependence on the current speed, favouring the B-DRIFT forecast for both stronger and weaker distributions. The $S(t)$ percentage difference between B-SSHG-DRIFT and B-DRIFT revealed the same dependence on the current speed as for $D(t)$.

The B-OSCAR-DRIFT and B-DRIFT forecast skill differences were similarly investigated (not shown) and the $D(t)$ percentage difference revealed no dependence on the current speed.

Table 8: Summary of Lagrangian metric statistics for different decorrelation length scale. Bold values denote that the difference between the original 100km experiments and the changed decorrelation length experiments are in significance ($p < 0.05$). (*) denotes significance at $p < 0.1$.

Metric	B-DRIFT [50]	B-SSHG-DRIFT [50]	B-DRIFT [150]	B-SSHG-DRIFT [150]
$\hat{D}(24)$ (km)	8.4 (6.6)	8.3 (6.5)	10.2 (9.0)	9.5 (7.3)
$D_{Linear}(0..96)$ (km/day)	**7.3 (5.3)** *	**7.0 (6.1)**	8.9 (6.6)	8.1 (6.1)
$AD(24)$ $(Degrees)$	7 ± 52	10 ± 52	7 ± 59	11 ± 60
$S(72)$ $n = 1$	0.4 [82%]	**0.43 [85%]**	0.32 [77%]	0.36 [77%]
$S(72)$ $n = 2$	0.66 [94%]	**0.67 [95%]**	0.60 [92%]	0.62 [94%]

Further to the mean current we also considered a dependence on the velocity variance (a measure of turbulence) and latitude (less than and greater than -10^o), both of which showed no significance between distributions.

3.4. Sensitivity to assimilation parameters

3.4.1. Decorrelation length scale sensitivity

A vital component of the data assimilation system is the choice of the decorrelation length scale in the initial condition background error covariance matrix, which determines the spread of influence for the assimilated data. The length scale was chosen as 100km, the average Rossby Radius. Four additional experiments were performed to investigate whether the results were sensitive to changes in this length scale. The first two represented assimilating B-DRIFT and B-SSHG-DRIFT with a decorrelation length scale of 50 km (decreasing by half the original length scale) and the second two with a scale of 150 km (increasing by half the original length scale).

Decreasing the decorrelation length scale by 50 km increased Lagrangian predictability for both B-SSHG-DRIFT and B-DRIFT experiments (Table

8). The statistical significance of this increase varied between the two experiments and different metrics (Bold in Table 8). Increasing the decorrelation length scale by 50 km slightly decreased Lagrangian predictability for both B-SSHG-DRIFT and B-DRIFT experiments in almost every Lagrangian metrics. However, this slight decrease across all metrics was not significant ($p > 0.25$). When decreasing and increasing the decorrelation length scale, for all metrics the difference between B-DRIFT and B-SSHG-DRIFT distributions remained insignificant. Therefore, the results presented here were robust to changes in background error decorrelation length scales by $\pm$ 50 km.

3.4.2. Drifter velocity observation error sensitivity

Another critical component of the data assimilation system is the choice observation error determining the weight given to the observations as compared to the background in the assimilation. Two additional experiments were performed to investigate the sensitivity of the drifter velocities error. Here, the drifter velocities errors in B-DRIFT and B-SSHG-DRIFT were doubled to 0.08 m/s.

The increased error did not significantly change Lagrangian predictability for both B-SSHG-DRIFT and B-DRIFT. When the drifter velocities error was doubled the difference between B-DRIFT and B-SSHG-DRIFT remained insignificant. Therefore, the results presented here were robust to doubling the drifter velocities error.

4. Discussion

The assimilation of drifter velocities improves the sea surface height forecast skill locally. The positive impact of assimilating drifter inferred velocities with a 4D-Var assimilation system on model SSH has been previously studied by Carrier et al. [9]. They describe two mechanisms for the adjustment on SSH from velocity assimilation acting through the adjoint and tangent linear components of a 4D-Var system. Firstly, a forcing of velocity in the adjoint model will propagate through to force the adjoint of the surface elevation via the geostrophic balance relationship. Secondly, the tangent linear model (initialized by the adjoint model) propagates this information forward in time as well as providing a forcing mechanism via the depth-integrated continuity equation. This effect of velocity assimilation on SSH (i.e. the multivariate characteristics in the model) is shown in Figure 3 demonstrating similar increments (posterior minus prior) produced for drifter and altimetry assimilation. Here the drifter coverage is too spare to improve domain wide statistics but can still influence large areas of the circulation such as creating eddies (Figure 5).

The forecast validation revealed that the assimilation and subsequent forecast of OSCAR currents performs worse than the B-SSHG forecast of OSCAR currents on average. From the analysis validation, the OSCAR forecast was initially closer to OSCAR observations than B-SSHG. However, ROMS is unable to maintain large domain-wide adjustments from the OSCAR assimilation as the forecast progresses. It is plausible that this was due to the frequency of the OSCAR observations, which was assimilated every five days while SSHG was assimilated daily. This difference in frequency

could then have a potentially large impact on the retention of skill.

For Lagrangian predictability, the addition of velocities inferred from drifters (either to a baseline assimilation of TS-SST (B) or B-SSHG) is shown on average to significantly improve Lagrangian predictability in the Angola Basin. A variety of skill metrics were used (see Table 2) to allow for robust conclusions. This is in agreement with previous work in the Gulf of Mexico [35, 9] and Mediterranean [37].

The addition of altimetry measuring sea surface height also significantly improves Lagrangian predictability on average, though only gaining half as much benefit as the addition of drifters. Superior improvements for drifters is unsurprising as even with highly chaotic trajectory forecasts, we would expect large improvements as the drifter trajectories are simulated in the vicinity of the assimilation.

Here OSCAR was assimilated for the first time in an advanced data assimilation system (4D-Var). Improvements in the Lagrangian predictability are roughly equivalent to the more traditional altimetry assimilation. The extra independent information in OSCAR such as the Ekman and Stommel shear dynamics [6] is not enough to provide improvements over just the sea surface height information, which was also assimilated four times more often than OSCAR. Aside from the reduced frequency of assimilation, it is also possible that without the multivariate balance of momentum, significant domain-wide adjustments of velocities are too extreme for ROMS to balance via the tangent linear and adjoint. Furthermore, the SSHG assimilation is notably effective at capturing the geostrophic currents through the multivariate characteristics of these models.

Sperrevik et al. [51] assimilated HR radar observations into a ROMS model of the Northern Norway coastline using IS-4DVAR. They also perform the same skill score metric utilised here for seven drifters and show a skill score improvement of 0.12 over a control run, 50% larger than that for OSCAR and SSHG in this study. Hoteit et al. [21] assimilated HR radar into a high-resolution MITgcm model of the San Diego Bay. They show the forecast exceeds persistence for up to 20 hours. It is hard to compare these results as they perform the assimilation in challenging area of highly ageostrophic conditions. Yaremchuk et al. [58] compared adjoint and adjoint-free 4D-Var systems assimilating 19 ADCP moorings. They found velocity forecast skill improved by 10-30% and persisted up to three days. In this study, OSCAR assimilation improves drifter velocity forecasts by just 13% as much as SSHG assimilation. In the only previous study of OSCAR assimilation, Santoki et al. [47] assimilated OSCAR via a nudging scheme into a model of the Indian Ocean. They found the RMSE of surface currents for 1-day and 5-day forecasts to be around 17 cms^{-1} and 19 cms^{-1} respectively thus, in four days the RMSE increases by 12%. Here, the average RMSE of drifter velocities over the entire four-day forecast is around 13 cms^{-1} with an average RMSE increase of around 13% in four days.

The combination of altimetry or OSCAR with drifter velocities does not on average significantly improve Lagrangian predictability upon the drifter inferred velocities alone. This result is unexpected as the combination of these observations has been previously shown to compliment each other [9]. For drifters in stronger currents, the combined altimetry and drifter assimilation is more likely to improve Lagrangian predictably by as much as 10% in

the forecast as compared to assimilating just the drifters alone. Conversely, for the drifters in weaker currents, the combination is actually more likely to degrade Lagrangian predictability by as much as 20%.

The sampling of the satellite observing system could be the cause of this the distinction. Stronger currents with a larger kinetic energy usually act on larger scales, which are better sampled by the satellite inferred geostrophic currents. Weaker currents on the other hand usually act on smaller scales better sampled by the drifters. Therefore, the assimilation of drifter could produce a better forecast in weaker currents. Besides the sampling accuracy, the variable coverage of a satellite observing system could also reduce skill. Berta et al. [4] used this to explain the variance in skill scores in the Gulf of Mexico when using Aviso geostrophic velocity estimates. Berta et al. [4] suggested that, since the altimetry coverage varies both temporally and spatially periods of low coverage could correspond to lower skill scores. Therefore, in areas of low coverage, the drifter inferred velocities are combined with an altimetry derived geostrophic current that is not accurate, degrading the performance of trajectory forecast skill. This issue is directly related to the utilisation of the gridded altimetry (SSHG) over the use of the along track altimetry (where low coverage areas would simply apply no assimilation at all). SSHG maps are an interpolated product and thus contain some estimate of the error covariance used to spread the information [36]. There are no prior criteria for the choice of altimetry product and the impact between gridded and along track assimilation of altimetry has not been directly quantified.

The assumptions that relate to the 4D-Var system are uncertain. The background and observational error covariance matrices determine the rel-

ative weighting of background and observational information in producing the optimal analysis, yet the construction of such matrices are subject to much ambiguity. This construction requires information on the background and observational error statistics and the scales of influence that are both uncertain. For example, da Rocha Fragoso et al. [13] determined the decorrelation length scale as a compromise between semivariogram analysis, the length scales of the main dynamic features of the studied region (Rossby radius of deformation), the model resolution, and subjective adjustment to optimise the performance of 4D-Var. The simplification of physics in the tangent linear/adjoint models could restrict the propagation of ageostrophic modes and multivariate characteristics established from dynamical balance relationships. However Sperrevik et al. [51] have previously shown that even in the presence of ageostrophic forcing ROMS 4D-Var can perform well.

Some of the results have been shown to be sensitive to the decorrelation length scale. For B-DRIFT and B-SSHG-DRIFT, Lagrangian predictability is significantly improved when reducing the length-scale by 50km. The smaller decorrelation length scale reduces the filtering effect on the smaller scales captured by the drifter [26], and thus local velocities are improved. Nevertheless, the difference between B-DRIFT and B-SSHG-DRIFT remain insignificant. None of the results were sensitive to doubling of the drifter velocity observation error.

5. Conclusion

Here, for the first time, we quantified the relative importance of assimilating combinations of altimetry, OSCAR and drifter observations for ocean

current forecasts. We achieve this by directly comparing the addition of either altimetry, OSCAR velocities, drifter inferred velocities and combinations of the three to a set of baseline observations assimilated into the ROMS 4D-Var system.

The assimilation system was first validated through cost function analysis and the J_{fit} metric representing the fit of the observations to the model analysis within one standard deviation of the observation error. The cost function reduced by 93% on average in all experiments reaching the asymptote by 25 iterations. For all experiments assimilating altimetry, the SSHG J_{fit} reduced below 1 improving against the baseline assimilation by approximately 70% on average. Similarity for all experiments assimilating OSCAR, the OSCAR velocities J_{fit} reduced below 1. For all experiments assimilating drifters, the drifter velocities J_{fit} laid close to 1. Therefore, we can conclude the assimilation system was correctly fitting all observations within observational error bounds.

The forecast skill was also assessed. The forecasts maintained perturbations from the assimilation system and exhibited an increased forecast skill from the assimilation system over four days. Interestingly, the domain-wide OSCAR velocities were best reproduced in the forecast by altimetry assimilation and not by the OSCAR assimilation itself. It is likely that the frequency of the OSCAR assimilation (every five days) has a detrimental impact on the performance as compared to the daily assimilated altimetry. We also showed that assimilating relatively few drifters can influence the locations of eddies as large 200 km.

Trajectory forecasts were computed for each observed drifter for every

forecast cycle, and four different Lagrangian predictability metrics were used for robustness. Drifter velocity assimilation is shown on average to significantly improve Lagrangian predictability of 4 different metrics in line with previous studies [37, 35, 9]. OSCAR assimilation only improves Lagrangian predictability as much as altimetry and only by half as much as the drifter assimilation.

A surprising finding is that when assimilating the combination of either altimetry or OSCAR and drifter velocities the Lagrangian predictability may degrade just as equally as improve compared to the assimilation of drifter velocities alone, and on average these combinations do not significantly improve the Lagrangian predictability.

The dependence of this degradation or improvement to the mean current was investigated. For the assimilation of altimetry combined with drifters, it is found in stronger currents the combination is more likely to increase (15%) the probability of improvement in the trajectory forecast. Conversely, for weak currents, a combination is more likely to decrease the probability of improvement. This distinction is thought to be attributed to the drifter observations ability to sample more effectively the smaller scales associated with weaker currents as compared to the variable sampling and coverage of the altimetry.

This study adds further support for the role of drifter data in an assimilation system. However, caution should be exercised when combining this information with other data.

Acknowledgements

This work was supported by the Natural Environment Research Council. The altimeter products were produced by Ssalto/Duacs and distributed by Aviso, with support from Cnes (http://www.aviso.altimetry.fr/duacs/).

[1] Anderson, D., Sheinbaum, J., Haines, K., 1996. Data assimilation in ocean models. Rep. Prog. Phys. 59, 1209–1266.

[2] Bauer, P., Thorpe, A., Brunet, G., sep 2015. The quiet revolution of numerical weather prediction. Nature 525 (7567), 47–55.

[3] Berta, M., Griffa, A., Magaldi, M. G., Özgökmen, T. M., Poje, A. C., Haza, A. C., Josefina Olascoaga, M., 2015. Improved surface velocity and trajectory estimates in the Gulf of Mexico from Blended satellite altimetry and drifter data. Journal of Atmospheric and Oceanic Technology 32 (10), 1880–1901.

[4] Berta, M., Griffa, A., Magaldi, M. G., Özgökmen, T. M., Poje, A. C., Haza, A. C., Josefina Olascoaga, M., oct 2015. Improved surface velocity and trajectory estimates in the Gulf of Mexico from Blended satellite altimetry and drifter data. Journal of Atmospheric and Oceanic Technology 32 (10), 1880–1901.
URL http://journals.ametsoc.org/doi/10.1175/JTECH-D-14-00226.1

[5] Boisribert, C., Virdin, J., 2008. Sub-Saharan Africa Region. Tech. rep., The World Bank.

[6] Bonjean, F., Lagerloef, G. S. E., oct 2002. Diagnostic model and analysis of the surface currents in the tropical Pacific Ocean. Journal of Physical Oceanography 32 (10), 2938–2954.
URL http://journals.ametsoc.org/doi/abs/10.1175/1520-0485{\%}282002{\%}29032{\%}3C2938{\%}3ADMAAOT{\%}3E2.0.CO{\%}3B2

[7] Broquet, G., Edwards, C. A., Moore, A. M., Powell, B. S., Veneziani, M., Doyle, J. D., oct 2009. Application of 4D-Variational data assimilation to the California Current System. Dynamics of Atmospheres and Oceans 48 (1-3), 69–92.

[8] Carrier, M. J., Ngodock, H., Smith, S., Jacobs, G., Muscarella, P., Ozgokmen, T., Haus, B., Lipphardt, B., apr 2014. Impact of Assimilating Ocean Velocity Observations Inferred from Lagrangian Drifter Data Using the NCOM-4DVAR*. Monthly Weather Review 142 (4), 1509–1524.
URL http://journals.ametsoc.org/doi/abs/10.1175/MWR-D-13-00236.1

[9] Carrier, M. J., Ngodock, H. E., Muscarella, P., Smith, S., mar 2016. Impact of Assimilating Surface Velocity Observations on the Model Sea Surface Height Using the NCOM-4DVAR*. Monthly Weather Review 144 (3), 1051–1068.
URL http://journals.ametsoc.org/doi/10.1175/MWR-D-14-00285.1

[10] Chassignet, E. P., Hurlburt, H. E., Smedstad, O. M., Halliwell, G. R.,

Hogan, P. J., Wallcraft, A. J., Baraille, R., Bleck, R., 2007. The HYCOM (HYbrid Coordinate Ocean Model) data assimilative system. Journal of Marine Systems 65 (1-4 SPEC. ISS.), 60–83.

[11] Chelton, D. B., DeSzoeke, R. A., Schlax, M. G., El Naggar, K., Siwertz, N., 1998. Geographical variability of the first baroclinic Rossby radius of deformation. Journal of Physical Oceanography 28 (3), 433–460.
URL {\%}3CGoto

[12] Clifford, A. C., 1986. African Oil – Past, Present, and Future. In: Halbounty, M. (Ed.), Future Petroleum Provinces of the World. Vol. 131. World, Am, Assoc, Pet, Geol, Ch. 40, pp. 339–372.

[13] da Rocha Fragoso, M., de Carvalho, G. V., Soares, F. L. M., Faller, D. G., de Freitas Assad, L. P., Toste, R., Sancho, L. M. B., Passos, E. N., Bck, C. S., Reis, B., Landau, L., Arango, H. G., Moore, A. M., 2016. A 4D-variational ocean data assimilation application for Santos Basin, Brazil. Ocean Dynamics, 1–16.
URL http://www.scopus.com/inward/record.url?eid=2-s2.0-84957708778{\&}partnerID=40{\&}md5=d9d68c8c99a37d37fa9e6c31504ec79d

[14] Dee, D. P., Uppala, S. M., Simmons, A. J., Berrisford, P., Poli, P., Kobayashi, S., Andrae, U., Balmaseda, M. A., Balsamo, G., Bauer, P., Bechtold, P., Beljaars, A. C. M., van de Berg, L., Bidlot, J., Bormann, N., Delsol, C., Dragani, R., Fuentes, M., Geer, A. J., Haimberger, L., Healy, S. B., Hersbach, H., Hólm, E. V., Isaksen, L., Kållberg, P., Köhler, M., Matricardi, M., McNally, A. P., Monge-Sanz, B. M.,

Morcrette, J.-J., Park, B.-K., Peubey, C., de Rosnay, P., Tavolato, C., Thépaut, J.-N., Vitart, F., apr 2011. The ERA-Interim reanalysis: configuration and performance of the data assimilation system. Quarterly Journal of the Royal Meteorological Society 137 (656), 553–597.
URL http://doi.wiley.com/10.1002/qj.828

[15] Denamiel, C., Budgell, W. P., Toumi, R., feb 2013. The Congo River plume: Impact of the forcing on the far-field and near-field dynamics. Journal of Geophysical Research: Oceans 118 (2), 964–989.
URL http://doi.wiley.com/10.1002/jgrc.20062

[16] Dombrowsky, E., Bertino, L., Brassington, G., Chassignet, E., Davidson, F., Hurlburt, H., Kamachi, M., Lee, T., Martin, M., Mei, S., Tonani, M., sep 2009. GODAE Systems in Operation.
URL http://tos.org/oceanography/article/godae-systems-in-operation

[17] Dorofeev, V. L., Korotaev, G. K., jan 2004. Assimilation of the data of satellite altimetry in an eddy-resolving model of circulation of the Black Sea. Physical Oceanography 14 (1), 42–56.
URL http://link.springer.com/10.1023/B:POCE.0000025369.39845.c3

[18] Fukumori, I., Raghunath, R., Fu, L. L., Chao, Y., nov 1999. Assimilation of TOPEX/Poseidon altimeter data into a global ocean circulation model: How good are the results? Journal of Geophysical Research-Oceans 104 (C11), 25647–25665.
URL http://doi.wiley.com/10.1029/1999JC900193

[19] Good, S. A., Martin, M. J., Rayner, N. A., dec 2013. EN4: Quality controlled ocean temperature and salinity profiles and monthly objective analyses with uncertainty estimates. Journal of Geophysical Research: Oceans 118 (12), 6704–6716.
URL http://doi.wiley.com/10.1002/2013JC009067

[20] Griffa, A., Piterbarg, L. I., Özgökmen, T., 2004. Predictability of Lagrangian particle trajectories: Effects of smoothing of the underlying Eulerian flow. Journal of Marine Research 62 (1), 1–35.

[21] Hoteit, I., Cornuelle, B., Kim, S. Y., Forget, G., Köhl, A., Terrill, E., oct 2009. Assessing 4D-VAR for dynamical mapping of coastal high-frequency radar in San Diego. Dynamics of Atmospheres and Oceans 48 (1-3), 175–197.
URL http://linkinghub.elsevier.com/retrieve/pii/S0377026508000717

[22] Johnson, E. S., Bonjean, F., Lagerloef, G. S. E., Gunn, J. T., Mitchum, G. T., apr 2007. Validation and Error Analysis of OSCAR Sea Surface Currents. Journal of Atmospheric and Oceanic Technology 24 (4), 688–701.
URL http://journals.ametsoc.org/doi/abs/10.1175/JTECH1971.1

[23] Lahoz, W., Khattatov, B., Menard, R., 2010. Data Assimilation and Information. In: Lahoz, W., Khattatov, B., Menard, R. (Eds.), Data Assimilation: Making Sense of Observations, 1st Edition. Springer-Verlag Berlin Heidelberg, Berlin, Ch. 1, pp. 3–12.

[24] Lapidus, L., Seinfeld, J. H. (Eds.), 1971. 4 Predictor-Corrector Methods. Vol. 74.

[25] Liu, Y., Weisberg, R. H., sep 2011. Evaluation of trajectory modeling in different dynamic regions using normalized cumulative Lagrangian separation. Journal of Geophysical Research 116 (C9), C09013.
URL http://doi.wiley.com/10.1029/2010JC006837

[26] Liu, Y., Weisberg, R. H., Vignudelli, S., Mitchum, G. T., 2014. Evaluation of altimetry-derived surface current products using Lagrangian drifter trajectories in the eastern Gulf of Mexico. Journal of Geophysical Research-Oceans 119 (5), 2827–2842.
URL {\%}3CGoto

[27] Lumpkin, R., Oz Okmen, T., Centurioni, L., 2017. Advances in the Application of Surface Drifters. Annu. Rev. Mar. Sci 9, 59–81.
URL www.annualreviews.org/doi/10.1146/annurev-marine-010816-060641

[28] Massey Jr, F. J., 1951. The Kolmogorov-Smirnov test for goodness of fit. Journal of the American statistical Association 46 (253), 68–78.
URL http://www.jstor.org/stable/2280095http://www.jstor.org/http://www.jstor.org/action/showPublisher?publisherCode=astata.

[29] Meybeck, M., Ragu, A., dec 2012. GEMS-GLORI world river discharge database.
URL https://doi.pangaea.de/10.1594/PANGAEA.804574

[30] Mogensen, K., Balmaseda, M. A., Weaver, A., 2012. The NEMOVAR ocean data assimilation system as implemented in the ECMWF ocean analysis for System 4. Tech. rep., ECMWF, Toulouse.

[31] Molcard, A., Griffa, A., Özgökmen, T. M., jan 2005. Lagrangian data assimilation in multilayer primitive equation ocean models. Journal of Atmospheric and Oceanic Technology 22 (1), 70–83.
URL http://journals.ametsoc.org/doi/abs/10.1175/JTECH-1686.1

[32] Molcard, A., Piterbarg, Griffa, Özgökmen, Mariano, 2003. Assimilation of drifter observations for the reconstruction of the Eulerian circulation field. ... Oceans (19782012 ... 108 (C3), 3056.
URL http://doi.wiley.com/10.1029/2001JC001240http://doi.wiley.com/10.1029/2001JC001240{\%}5Cnhttp://onlinelibrary.wiley.com/doi/10.1029/2001JC001240/full

[33] Moore, A. M., Arango, H. G., Broquet, G., Edwards, C., Veneziani, M., Powell, B., Foley, D., Doyle, J. D., Costa, D., Robinson, P., oct 2011. The Regional Ocean Modeling System (ROMS) 4-dimensional variational data assimilation systems: Part II Performance and application to the California Current System. Progress in Oceanography 91 (1), 50–73.
URL http://www.sciencedirect.com/science/article/pii/S0079661111000504

[34] Moore, A. M., Arango, H. G., Broquet, G., Powell, B. S., Weaver, A. T., Zavala-Garay, J., oct 2011. The Regional Ocean Modeling

System (ROMS) 4-dimensional variational data assimilation systems: Part I System overview and formulation. Progress in Oceanography 91 (1), 34–49.
URL http://www.sciencedirect.com/science/article/pii/S0079661111000516

[35] Muscarella, P., Carrier, M. J., Ngodock, H., Smith, S., Lipphardt, B. L., Kirwan, A. D., Huntley, H. S., 2015. Do Assimilated Drifter Velocities Improve Lagrangian Predictability in an Operational Ocean Model? Monthly Weather Review 143 (5), 1822–1832.
URL http://journals.ametsoc.org/doi/pdf/10.1175/MWR-D-14-00164.1

[36] Ngodock, H., Carrier, M., Souopgui, I., Smith, S., Martin, P., Muscarella, P., Jacobs, G., 2016. On the direct assimilation of along-track sea-surface height observations into a free-surface ocean model using a weak constraints four-dimensional variational (4D-Var) method. Quarterly Journal of the Royal Meteorological Society 142 (695), 1160–1170.

[37] Nilsson, J. A. U., Dobricic, S., Pinardi, N., Poulain, P. M., Pettenuzzo, D., 2012. Variational assimilation of Lagrangian trajectories in the Mediterranean ocean Forecasting System. Ocean Science 8 (2), 249–259.
URL www.ocean-sci.net/8/249/2012/

[38] Nodet, M., feb 2006. Variational assimilation of Lagrangian data in oceanography. Inverse Problems 22 (1), 245–263.
URL http://arxiv.org/abs/0804.1137

[39] Özgökmen, T. M., Molcard, A., Chin, T. M., Piterberg, L. I., Griffa, A., 2003. Assimilation of drifter observations in primitive equation models of midlatitude ocean circulation. Journal of Geophysical Research: Oceans 108 (7), 31–1.

[40] Pazos, R. L., Mayra, Lumpkin, R., Pazos., M., 2007. Measuring surface currents with Surface Velocity Program drifters: the instrument, its data, and some recent results. In: Griffa, A., Kirwan, A. D., Mariano, A. J., Ozgokmen, T., Rossby, T. (Eds.), Lagrangian Analysis and Prediction of Coastal and OCean Dynamics. Cambridge University Press, pp. 39–67.
URL http://dx.doi.org/10.1017/CBO9780511535901.003

[41] Pérez, M. E., Charles, C. D., Berger, W. H., 2001. Late quaternary productivity fluctuations off Angola: evidence from benthic foraminifers, site 1079. Proceedings of the Ocean Drilling Program, Scientific Results 175 (July 2000), 1–19.

[42] Poje, A. C., Ozgökmen, T. M., Lipphardt, B. L., Haus, B. K., Ryan, E. H., Haza, A. C., Jacobs, G. A., Reniers, A. J. H. M., Olascoaga, M. J., Novelli, G., Griffa, A., Beron-Vera, F. J., Chen, S. S., Coelho, E., Hogan, P. J., Kirwan, A. D., Huntley, H. S., Mariano, A. J., sep 2014. Submesoscale dispersion in the vicinity of the Deepwater Horizon spill. Proceedings of the National Academy of Sciences of the United States of America 111 (35), 12693–8.
URL http://www.ncbi.nlm.nih.gov/pubmed/25136097http://www.pubmedcentral.nih.gov/articlerender.fcgi?artid=

PMC4156713http://www.scopus.com/inward/record.url?eid=2-s2.0-84907228013{\&}partnerID=tZOtx3y1{\%}5Cnhttp://www.ncbi.nlm.nih.gov/pubmed/24982135{\%}5Cnhttp://doi

[43] Rabier, F., oct 2005. Overview of global data assimilation developments in numerical weather-prediction centres. Quarterly Journal of the Royal Meteorological Society 131 (613), 3215–3233.
URL http://doi.wiley.com/10.1256/qj.05.129

[44] Reynolds, R. W., Smith, T. M., Liu, C., Chelton, D. B., Casey, K. S., Schlax, M. G., nov 2007. Daily high-resolution-blended analyses for sea surface temperature. Journal of Climate 20 (22), 5473–5496.
URL http://journals.ametsoc.org/doi/abs/10.1175/2007JCLI1824.1

[45] Roberts, J., Roberts, T. D., 1978. Use of the Butterworth Low-Pass Filter for Oceanographic Data. Journal of Geophysical Research: Oceans 83 (8), 5510–5514.

[46] Salman, H., Kuznetsov, L., Jones, C. K. R. T., Ide, K., apr 2006. A Method for Assimilating Lagrangian Data into a Shallow-Water-Equation Ocean Model. Monthly Weather Review 134 (4), 1081–1101.
URL http://journals.ametsoc.org/doi/abs/10.1175/MWR3104.1

[47] Santoki, M., George, S., Sharma, R., Joshipura, K. N., Basu, S., may 2013. Assimilation of satellite-derived ocean surface current in an Indian Ocean circulation model. Remote Sensing Letters 4 (5), 475–484.

URL http://www.tandfonline.com/doi/abs/10.1080/2150704X.2012.750036

[48] Sharma, N., Brickley, P., Owen, G., Coholan, P., 2010. Use of air-deployed drogued drifting buoys for oil spill tracking. In: MTS/IEEE Seattle, OCEANS 2010.

[49] Shchepetkin, A. F., McWilliams, J. C., 2005. The regional oceanic modeling system (ROMS): A split-explicit, free-surface, topography-following-coordinate oceanic model. Ocean Modelling 9 (4), 347–404.

[50] Smith, S., Carrier, M., Ngodock, H., Shriver, J., Muscarella, P., Penta, H., Carroll, S., 2015. Validation Test Report for the Navy Coastal Ocean Model Four-Dimensional Variational Assimilation (NCOM 4DVAR) System Version 1.0. Tech. rep., Naval Research Laboratory.

[51] Sperrevik, A. K., Christensen, K. H., Röhrs, J., 2015. Constraining energetic slope currents through assimilation of high-frequency radar observations. Ocean Science 11 (2), 237–249.
URL www.ocean-sci.net/11/237/2015/

[52] Stramma, L., Schott, F., 1999. The mean flow field of the tropical Atlantic Ocean. Deep-Sea Research II 46, 279–303.

[53] Thyng, K. M., Hetland, R. D., 2014. TracPy : Wrapping the Fortran Lagrangian trajectory model TRACMASS. Proceedings of the 13th Python in Science Conference (Scipy 2014) (Scipy), 85–90.

[54] Vorosmarty, C., Fekete, B. M., Tucker, B., 1998. Global River Discharge,

1807-1991, V. 1.1 (RivDIS).
URL http://dx.doi.org/10.3334/ORNLDAAC/199

[55] Warner, J. C., Sherwood, C. R., Arango, H. G., Signell, R. P., 2005. Performance of four turbulence closure models implemented using a generic length scale method. Ocean Modelling 8 (1-2), 81–113.

[56] White, R. H., Toumi, R., 2014. River flow and ocean temperatures: The Congo River. Journal of Geophysical Research: Oceans 119 (4), 2501–2517.
URL http://dx.doi.org/10.1002/2014JC009836

[57] Willis, J. K., Roemmich, D., Cornuekke, B., 2004. Interannual variability in upper ocean heat content, temperature, and thermosteric expansion on global scales. Journal of Geophysical Research 109, C12036.

[58] Yaremchuk, M., Martin, P., Koch, A., Beattie, C., 2016. Comparison of the adjoint and adjoint-free 4dVar assimilation of the hydrographic and velocity observations in the Adriatic Sea. Ocean Modelling 97, 129–140.

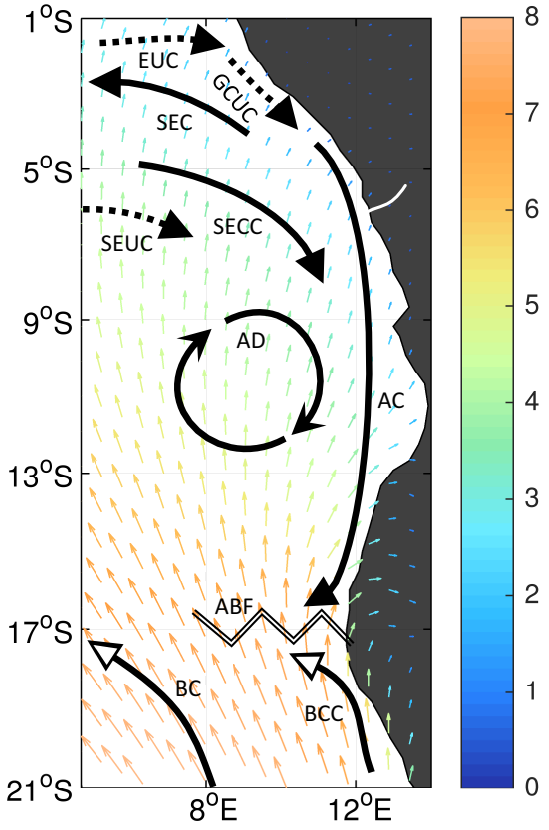

Figure 1: Schematic of all the major oceanographic features of the Angola Basin. Warm surface currents (solid lines with black arrowheads) are the South Equatorial Current (SEC), South Equatorial Counter Current (SECC), Angola Current (AC). Warm undercurrents (dashed lines with black arrowheads) are the Equatorial Undercurrent (EUC) and Gabon-Congo Undercurrent (GCUC). Cold surface currents (solid lines with white arrowhead) are; the Benguela Oceanic Current (BOC) and Benguela Coastal Current (BCC). Also shown, The Angola Dome (AD), the Angola-Benguela Front (ABF) and the Congo River (CR). Overlaid as vector velocities (m/s) are the ERA-I (JFM) averaged winds averaged over the study period. Adapted from Pérez et al. [41]

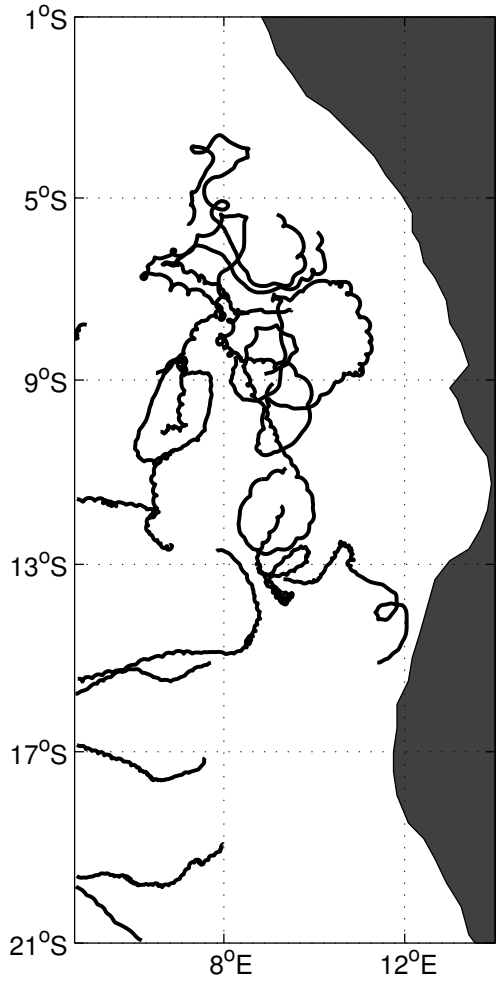

Figure 2: Location of all the drifters used throughout the study. A maximum of 4-16 drifter observations were simultaneously assimilated through each assimilation cycle.

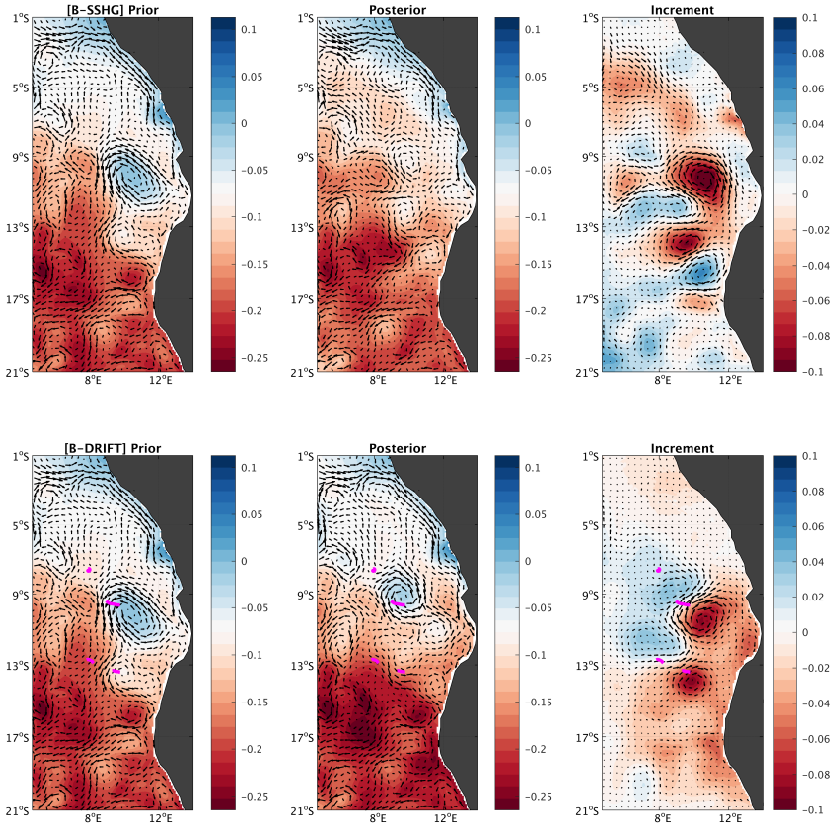

Figure 3: Column left to right: Prior (background forecast), posterior (updated forecast from the assimilation system) and increments (posterior minus prior) of model SSH averaged over the first assimilation cycle, 1st to 5th January. Overlaid are the model velocity vectors. Top to bottom: The B-SSGH experiment and B-DRIFT experiment. Highlighted in the B-DRIFT field in magenta (online version) / black (in print version) are the drifters available for assimilation in the first cycle.

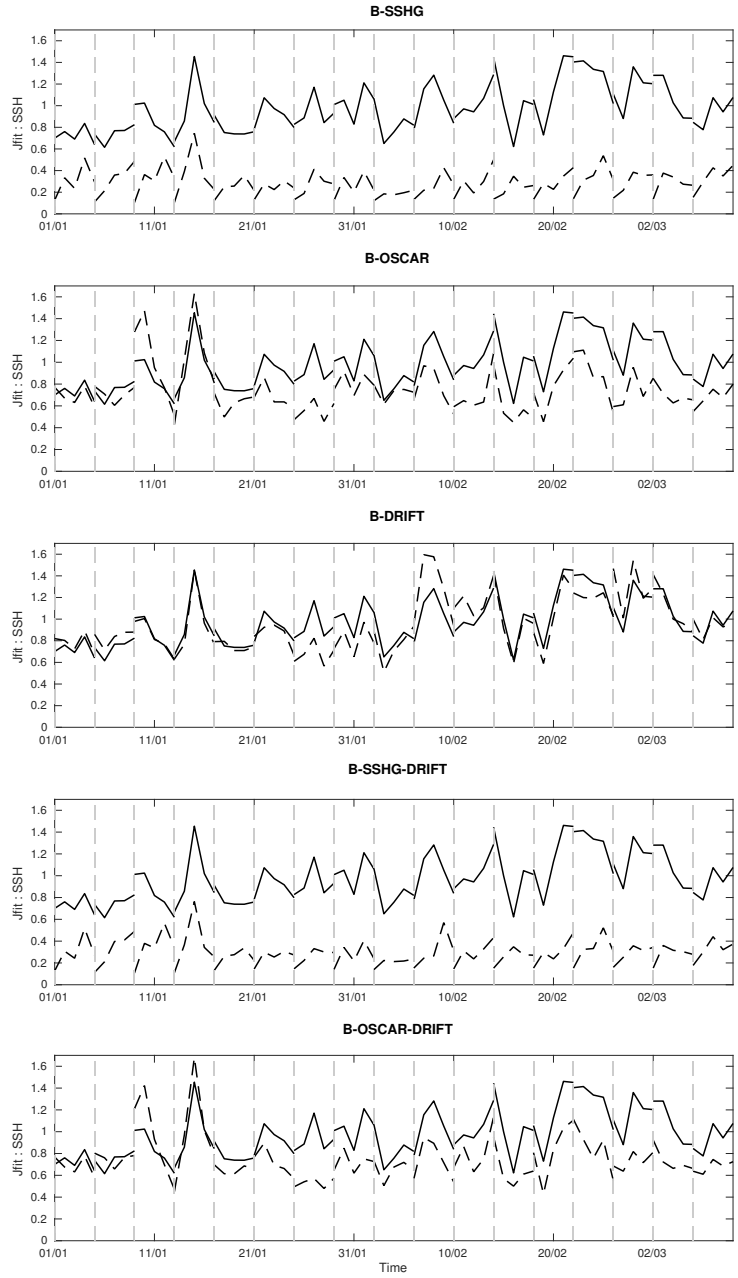

Figure 4: The SSHG J_{fit} time series for five experiments, B-SSHG , B-OSCAR, B-DRIFT, B-SSHG-DRIFT and B-OSCAR-DRIFT in dashed black lines. The bold black line in each figure represents the J_{fit} for experiment TS-SST the baseline for comparison.

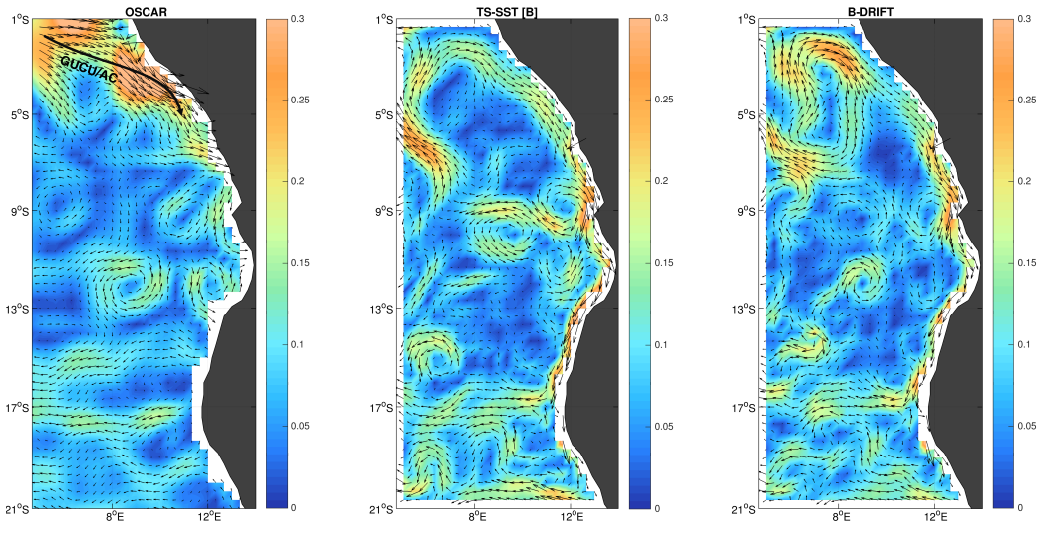

Figure 5: Ocean current speeds (m/s) and velocity vectors averaged over all forecast cycles (5th January-13th March) and the top 30 meters depth for OSCAR analysis, control (free run with no assimilation), TS-SST (B), and B-DRIFT. The GUCU is highlighted in the OSCAR analysis.

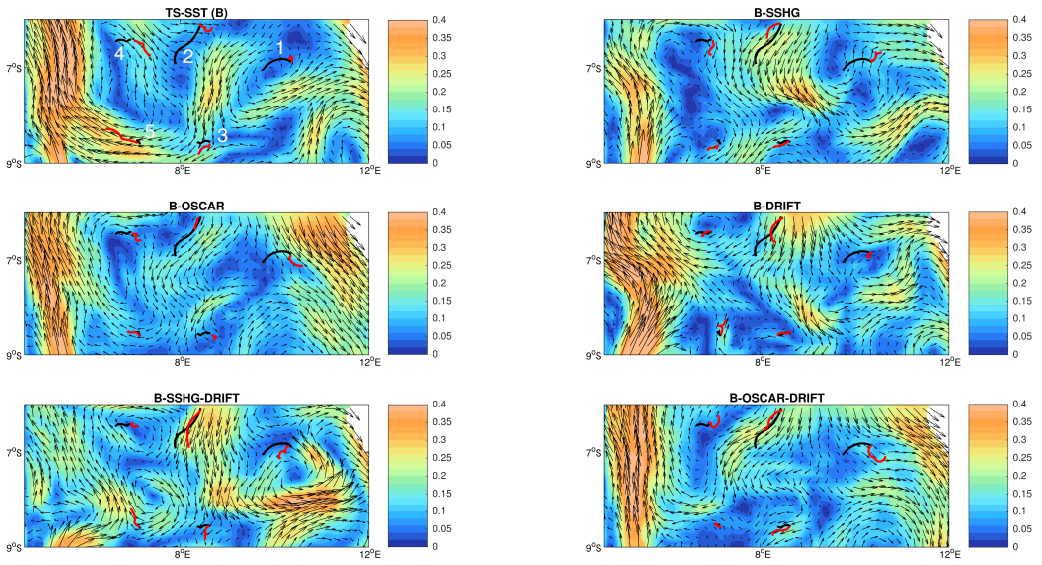

Figure 6: Ocean current speeds (m/s) and velocity vectors for a sub-section of the Angola Basin domain averaged over the four-day forecast from 22nd to 26th February 2013 for TS-SST (B), B-SHH, B-OSCAR, B-DRIFT, B-SSHG-DRIFT and B-OSCAR-DRIFT. Simulated float forecasts for each experiment within the sub-domain are shown as red lines (online version only) / black crosses (print version). Real observations of the drifters are shown as black lines. The labels 1-5 for each drifter is displayed in TS-SST (B)

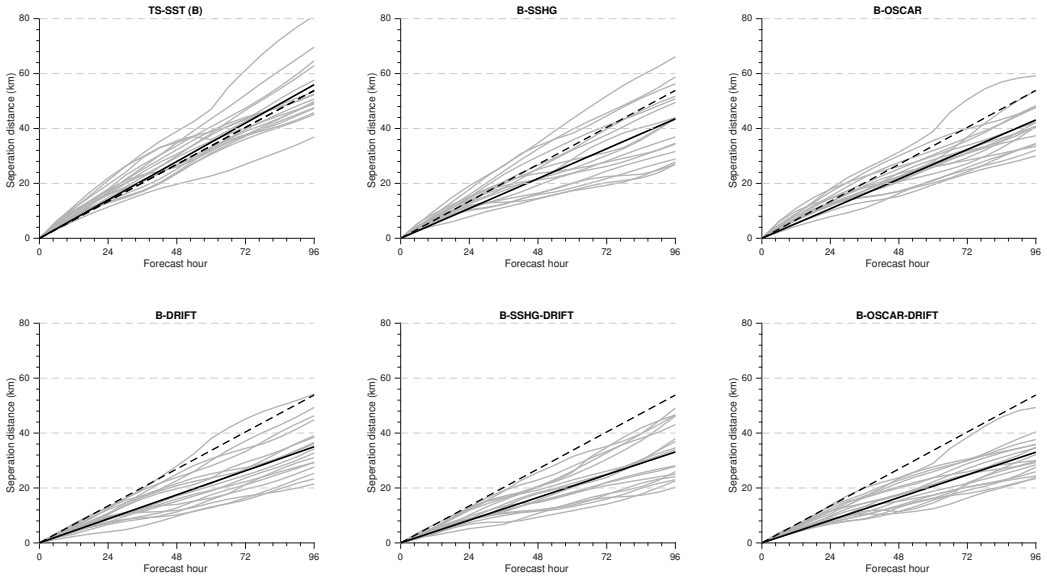

Figure 7: The average and spread of the growth rate in separation per day (km/day) for TS-SST (B), B-SSHG, B-OSCAR, B-DRIFT, B-SSHG-DRIFT and B-OSCAR-DRIFT. Each grey line represents the average separation over the entire domain (drifter averaged) within one forecast cycle. The black line represents the average over all drifters and forecasts. The dashed line shows the CONTROL (free run without assimilation) averaged over all drifters and forecasts for comparison.

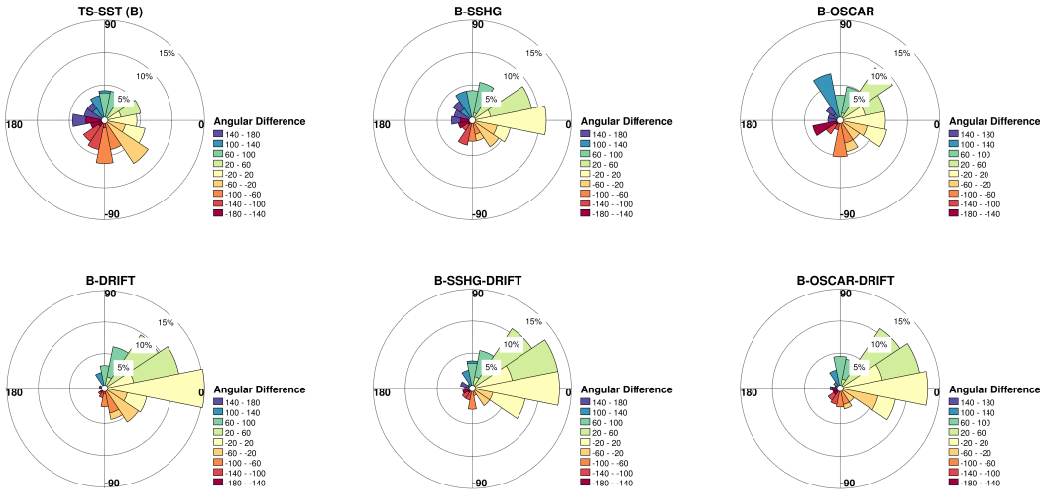

Figure 8: Wind roses of the spread of angular differences between each observed 24-hour drifter angle (the angle between the starting position and position at 24 hours) and 24-hour simulated trajectory angle for TS-SST (B), B-SSHG, B-OSCAR, B-DRIFT, B-SSHG-DRIFT and B-OSCAR-DRIFT.

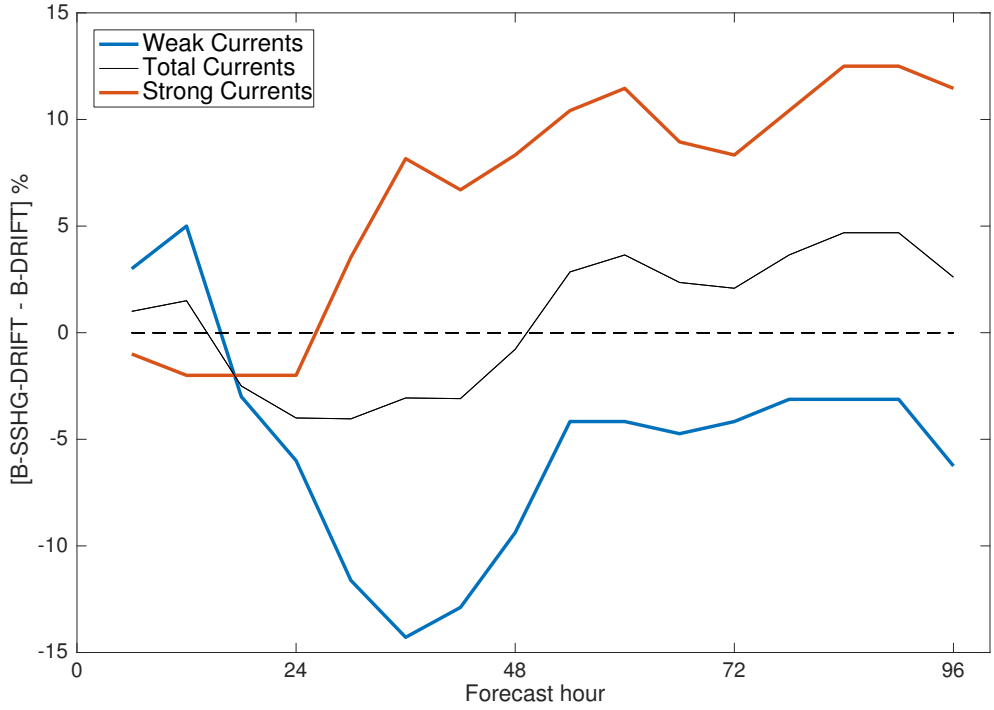

Figure 9: The positive to negative percentage difference of $D(t)$ between B-SSHG-DRIFT and B-DRIFT as a function of time. Positive values denote that the B-SSHG-DRIFT has a larger proportion of improved trajectory forecast than B-DRIFT. Conversely, a negative value denotes that B-DRIFT has a greater proportion of improved trajectory forecast than B-SSHG-DRIFT. The distributions of $D(t)$ are split into three categories; total, weaker and stronger currents based on the median of the observed drifter speed distribution (upper and lower 50%).